Extension and Validation of a Pointing Image Simulation for the CTA MST

Bachelorarbeit aus der Physik

Vorgelegt von

Martin Hein

12.08.2022

Erlangen Centre for Astroparticle Physics

Friedrich-Alexander-Universität Erlangen-Nürnberg

Betreuer: Prof. Dr. Christopher van Eldik

Abstract

The Cherenkov Telescope Array (CTA) observatory will consist of over 100 next generation telescopes constructed to detect Cherenkov light produced by very high energy gamma rays.
The knowledge about the exact observed location on the sky, i e. the telescope pointing direction, is crucial for a high angular resolution. An optical camera will be used on the Medium-Sized Telescopes (MST) for determining the pointing.
In terms of this thesis, the simulation and analysis framework of those pointing images will be expanded by including the simulation of the support structure of the Cherenkov camera and reference LEDs. The resulting simulated images are reproducing the real pointing images adequately.
Furthermore, a systematic offset in the spot extraction procedure is observed.
Lastly, the analysis shows an increasing precision in determining the camera center for increasing number of reference LEDs used for fitting a circle to them. Also, a symmetrical constellation of LEDs reduces the sensitivity of the fit to statistical uncertainties of individual LED positions.

Zusammenfassung

Das Cherenkov Telescope Array (CTA) Observatorium wird aus über 100 Teleskopen der nächsten Generation bestehen, konstruiert, um Cherenkov Licht zu detektieren, das durch hochenergetischen Gammastrahlen erzeugt wird.
Die Kenntnis über die genau beobachtete Position am Himmel, d. h. die Ausrichtung des Teleskops, ist essentiell für eine hohe Winkelauflösung. Eine optische Kamera wird an Medium-Sized Telescopes (MST) verwendet, um die Ausrichtung zu bestimmen.
Im Sinne dieser Abschlussarbeit werden das Simulations- und Analyseframework von solchen Ausrichgungsbildern um die Simulation des Tragwerkes der Cherenkov-Kamera und Referenz-LEDs erweitert. Die resultierenden simulierten Bilder resproduzieren adäquat echte Ausrichtungsbilder.
Des Weiteren is ein systematischer Offset im Spot-Extraction-Vorgang beobachtet worden.
Schließlich zeigt die Analyse eine steigende Präzision in der Bestimmung des Kamerazentrums für eine steigende Zahl an Referenz-LEDs, die zum Fitten eines Kreises dienen. Auch reduziert eine symmetrische Konstellation der LEDs die Empfindlickeit des Kreis-Fits auf statistische Unsicherheiten in den LED-Positionen.

Contents

1 Introduction

The fascinating thing about watching the night sky is, that each spot tells a different story. While we call every spot a star, we sometimes see shooting stars, which are rocks flying through our atmosphere. Now imagine, that these stars could indeed be whole galaxies, held together by massive black holes. We can not see those by our own eyes. That is why we build telescopes. They give us the ability to zoom into the universe and observe various events.
Those events reveal to us by sending out electromagnetic waves, photons, which are caught by the telescope's detectors. Each object sends out different spectra of light, giving us a clue what happens around that object. Stars for example emit thermal light in the spectrum from infrared to ultraviolet. Light with higher energies like X-rays and gamma-rays are not created by thermal processes. They can be produced e. g. by interaction of accelerated cosmic rays in matter.
Cosmic rays are particles like protons and atomic nuclei accelerated close to the speed of light and carry a very high amount of energy. Environments capable of accelerating particles to such energies are for example supernova remnants or black holes. The direct detection of cosmic rays does not deliver much information due to for instance deflection in cosmic magnetic fields. Since they can interaction with matter or magnetic fields near those cosmic ray accelerators, the developing gamma-rays can be observed, which allows tracing these acceleration mechanisms in the universe.[2]

1.1 Atmospheric particle showers

When cosmic gamma-ray photons hit the earth's atmosphere, they interact with the prevailing atomic nuclei. Due to the high energy of the gamma-rays, electron-positron pair production dominates. In further interaction, the electrons and positrons lose energy, mostly producing bremsstrahlung. This process repeats consistently, resulting in a cascade of highly energetic, charged particles, until the energy of the photons of bremsstrahlung is no longer sufficient to produce new electron-positron pairs. This is the shower maximum. In Figure 1 the principle idea of an atmospheric particle shower is shown.

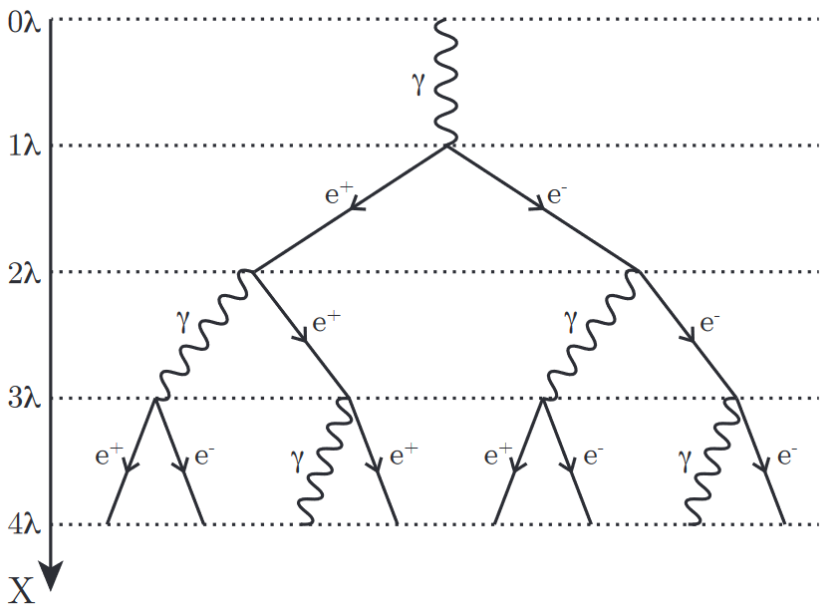

Figure 1: Schematic drawing of a gamma-ray shower in the atmosphere. It is a repeating process of electron-positron pair production and bremsstrahlung (Heitler, 1954)[4].[5]

The model suggests a duplication of all participating particles each pass through one collision length λ.

1.2 Cherenkov radiation

The high energetic charged particles in the showers move through the atmosphere with velocities greater than the local speed of light

$$c_{\text{loc}} = \frac{c}{n} \tag{1}$$

with the speed of light in vacuum c and the refractive index n of the traversed medium. As they pass by, surrounding molecules experience net polarization. This polarization propagates through the medium, leading to radiation of electromagnetic waves. This is called Cherenkov radiation, named after Pavel Cherenkov who first discovered this effect[7]. That Cherenkov light is radiated in a cone in the forward direction of the moving particles. Its opening angle θ, defined in equation 2, depends on the local speed of light and the velocity v of the particles from the shower.

$$\theta = \cos^{-1}\left(\frac{c_{\text{loc}}}{v}\right) \tag{2}$$

Assuming a constant gas composition of the atmosphere, the refractive index n is proportional to the density of the gas, which is proportional to the pressure of the gas. The pressure is a function of the height h above the ground. Thus, n changes with h, so the height of Cherenkov photon production influences the opening angle. The cone illuminates a circular area on the ground with a radius of $h \sin \theta$.
For gamma-rays of energies in the order of TeV the maximum of the shower develops at around 10 km above sea level with the Cherenkov angle of about 0.7°, illuminating a circle of radius in the order of 100 m depending on the height above sea level of the telescope.[9]

The challenge is to detect those light flashes which, viewed from the ground, have a duration in the order of nanoseconds. Imaging Air Cherenkov Telescopes (IACTs) are specifically designed for detecting those flashes. They are composed of large mirror surfaces, which are required in order to collect enough light from the faint signal of the Cherenkov cone. These mirrors then image the incident photons to specially designed Cherenkov cameras capable of measuring the nanosecond signal.

1.3 Cherenkov Telescope Array

The future Cherenkov Telescope Array (CTA) is an observatory consisting of many of those IACTs.
These will be the next generation telescopes to detect Cherenkov light [2]. Since cascades of photons with energies greater than 10 TeV are so rare, more than 100 telescopes in total will be placed to enlarge the effective detection area, which improves the chance of capturing them. The individual telescopes will be placed on each hemisphere, namely in La Palma and in Chile. The last location is suited for observing gamma-rays coming from the Milky Way itself.
CTA will consist of three classes of telescopes, illustrated in Figure 2, from Small-Sized Telescope (SST) over Medium-Sized Telescope (MST) to Large-Sized Telescope (LST). Each class will cover a specific interval of energy of the gamma-rays, with a combined spectrum from 20 GeV to 300 TeV.

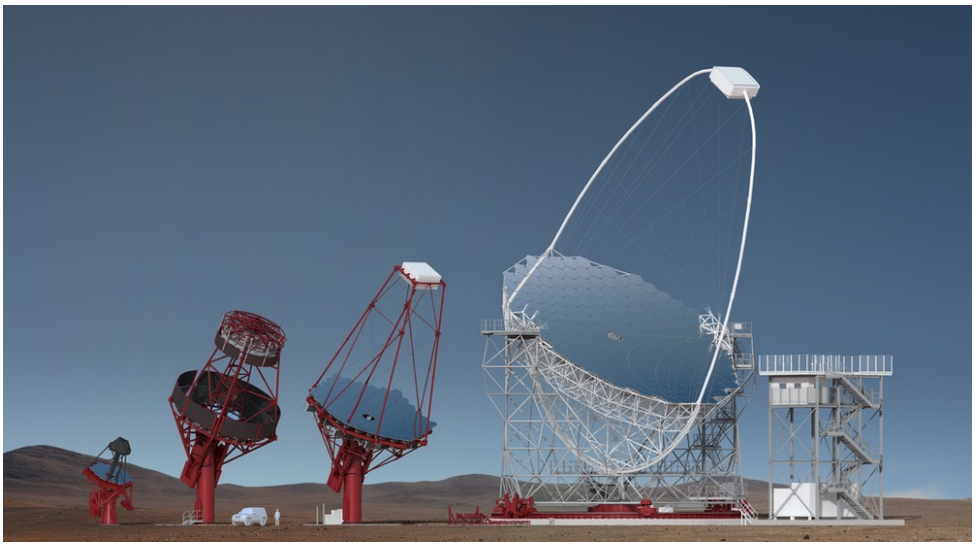

Figure 2: (from left to right) Illustration of prototype designs for Small-Sized Telescope (SST), two Medium-Sized Telescope (MST) and Large-Sized Telescope (LST).[2]

CTA will be the successor of prior experiments H.E.S.S., VERITAS and MAGIC and has the potential to improved energy range, sensitivity as well as angular resolution. The data taken by CTA will be accessible to the world-wide astronomical and particle physics community.

1.4 Telescope pointing

In order to be able to distinguish individual sources of radiation and precisely identify source locations, the pointing direction of the telescope must be known to a high accuracy. Therefore, the systematical error of pointing must be measured and corrected for. This can be done with the help of optical cameras that measure the star field and location of the Cherenkov camera. Thus, sagging of the camera mounting structure and mirror dishes due to their weight can be corrected.[1]

On the CTA telescopes, a wide field optical camera right at the center of the mirror dish will be installed. Testings of design and functionality are currently done on prototypes as well as on one of the two Major Atmospheric Gamma Imaging Cherenkov (MAGIC) telescopes (see Figure 3) in La Palma. Especially on the MAGIC telescope, an optical camera is mounted as described. This allows to collect data necessary to optimally construct and launch the CTA telescopes.

Requirement set by CTA is to get a pointing precision better than 7 arcsec per axis.

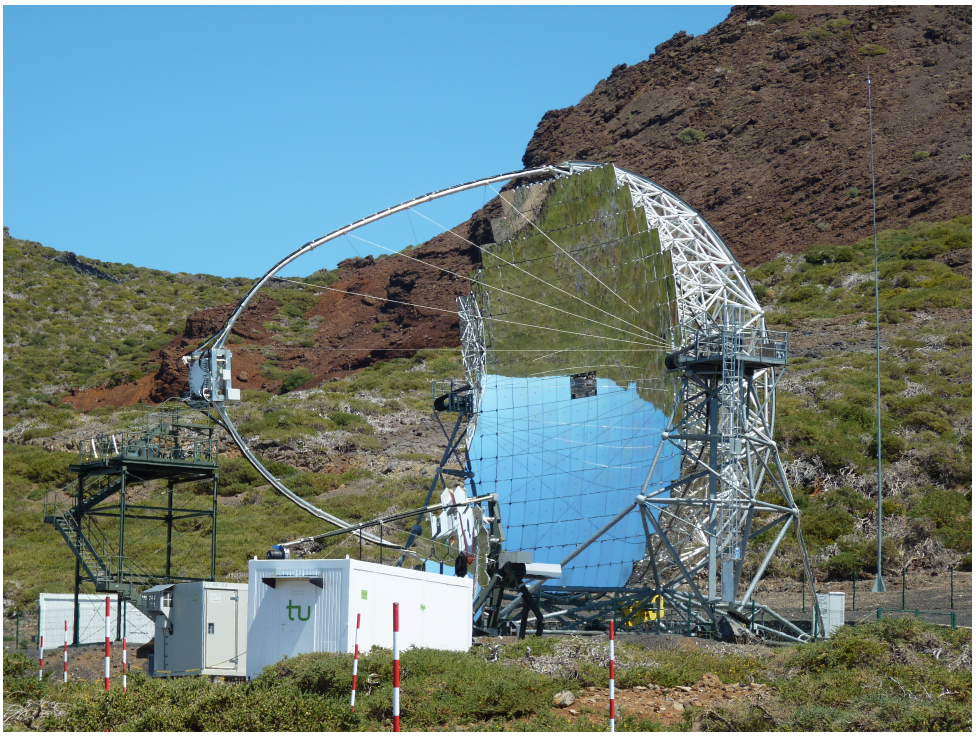

Figure 3: One of the Major Atmospheric Gamma Imaging Cherenkov (MAGIC) telescopes in La Palma with an optical camera for determining the telescope pointing mounted at the center of the mirror dish.[3]

1.5 Image simulations

In order to develop and study sophisticated analysis methods, it is convenient to simulate images of the pointing camera. By that, algorithms can be developed and easily be tested without running an actual telescope. Since CTA is currently being built, these algorithms can be developed and improved before even having a single image taken by the telescope. Since simulated images need to be validated, the images taken from the MAGIC telescope are used. As a consequence, simulations are created for MAGIC. The algorithms are then applied on the real and simulated images.

1.6 Software

The Offline MST telescope pointing pipeline prototype for CTA is a prototype data processing framework written in the programming language Python.[8] It provides a simulation framework designed for simulating the star field of pointing images, as well as analysis

tools including spot extraction algorithms and LED fitting methods.

In this thesis, the aim is to extend the simulation framework by including components of the telescope structure holding the Cherenkov camera in the simulation and analysis chain.
In a further step, the quality of the simulations needs to be analyzed by comparing them to real exposures. Finally, the results of the analysis algorithms will be studied under various conditions.

2 LED fitting in images taken on MAGIC

First, we need to take a close look at the exposure images taken by the pointing camera on the MAGIC telescope. An exemplary image can be seen in Figure 4.
It contains the Cherenkov camera and a part of its support structure. There are twelve reference LEDs placed on a circle around the detector. The barycenter of all LEDs defines the center of the Cherenkov camera by construction. Note, that four of the LEDs on MAGIC were not operational at the time of image taking.
A part of the night sky with stars is also visible around the camera structure.

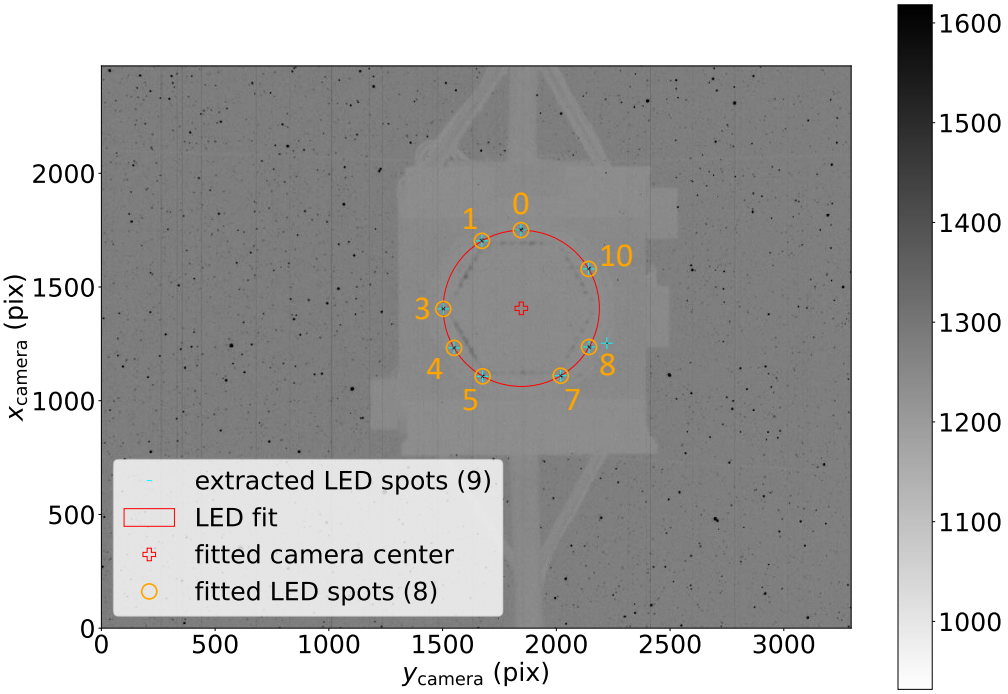

Figure 4: Image of the pointing camera with exposure duration of 15 s. It contains the night sky and the camera support structure with Cherenkov camera and reference LEDs arranged in a circle around. Spots on the camera structure detected by the spot extraction tool and the circle with its center position fitted to the identified LED spots by the LED fitting tool are shown. The LEDs are labeled from 0 to 10.

Since the simulation of the star field in pointing images has already been implemented in the framework, the focus in this work lies on modelling the camera support structure with

the reference LEDs. Therefore, we need to extract the position of each LED and analyze the intensity profile of those in real exposure images.

Extraction of LED positions

The spot extraction tool analyzes the image and provides the pixel coordinates of all spots that exceed a certain intensity threshold. Aiming to detect the reference LEDs, a mask is applied to only extract spots in the region of the camera body. It is still possible, that there are bright spots detected in this area, which are no LEDs. This can be seen in Figure 4.
The algorithm also determines the variance, which also represents the squared width of the spot, in x and y direction, as well as the total intensity. There are other values provided as well, which are redundant for this work.

LED fitting

After extracting the spots, the data is used to fit a circle, which is constructed by the LED positions, weighted with the intensity distribution of each spot. The fitting gets performed multiple times until the spots, that are further away from the fitted circle than some specified tolerance, get discarded, thus improving the accuracy of the fit. So, this functionality is useful to derive with LED spots only.

LED intensity profile

Now, the intensity profile of each individual LED can be analyzed. For each LED, the profile in x and y direction is considered separately.
The process described in the following is representatively shown for one LED in Figure 5.

The LEDs have a radius of about 4 pixels containing 68 % of the total intensity and a radius of about 7 pixels in total size.
A box of 31×31 pixels is laid around the extracted position. In that region, all row slices are summed up to map the two-dimensional intensity profile to one dimension, which also suppresses statistical fluctuations of the individual pixel values. This delivers the intensity profile in y direction. To obtain the profile in x direction, the column slices are summed up analogically.

The assumption is that the intensity profile per axis can be approximated by a Gaussian distribution. To verify this, a Gaussian curve following the equation

$$g(x) = a \cdot \frac{1}{\sqrt{2\pi\sigma^2}} \cdot \exp\left(-\frac{(x-\mu)^2}{2\sigma^2}\right) + t \tag{3}$$

is fitted. Here μ is the position of the center of the curve and σ is its width. The intensity distribution is not normalized, so a is multiplied as the scaling factor, which also represents the integral of the curve, and t is added as the offset, taking the intensity of the underground into account.
As can be seen in the Figure 5, the Gaussian curve does indeed approximate the intensity distribution in each direction. We can also compare the position μ and width σ from the fit with those found by the extraction software, as well as the total intensity a and the underground t from the fit. The underground around the LED is estimated by averaging the border values of the box. The comparison for the LED shown in Figure 5 is recorded in Table 1.

		x profile				y profile			
		extraction	Gaussian fit			extraction	Gaussian fit		
μ	(pix)	1236.30	1236.52	$\pm$	0.17	2143.83	2144.73	$\pm$	0.18
σ	(pix)	3.97	3.91	$\pm$	0.22	3.97	3.94	$\pm$	0.24
a	(pix)	288158.00	329214.80	$\pm$	2132.75	288158.00	330302.02	$\pm$	2320.52
t	(pix)	38587.67	37575.46	$\pm$	840.01	38539.50	37540.87	$\pm$	910.00

Table 1: Comparison between the fitting parameters and the corresponding values from the spot extractor for the profile per axis in Figure 5. The meaning of the parameters is explained in the paragraph above.

The position and width in both axis directions of the distribution do differ by less than 1 pix. However, the total intensity by the Gaussian fit differs about 14 % of the extracted intensity. The underground of the fit is by less than 1 % slightly lower than the underground estimated by averaging.
That can be explained visually in Figure 5. The Intensity at the center of the LED is not perfectly Gaussian distributed, resulting in a not optimal fit. Thus, the baseline is visibly pulled slightly below the background intensity. For now, approximation by a Gaussian distribution is perfectly fine.

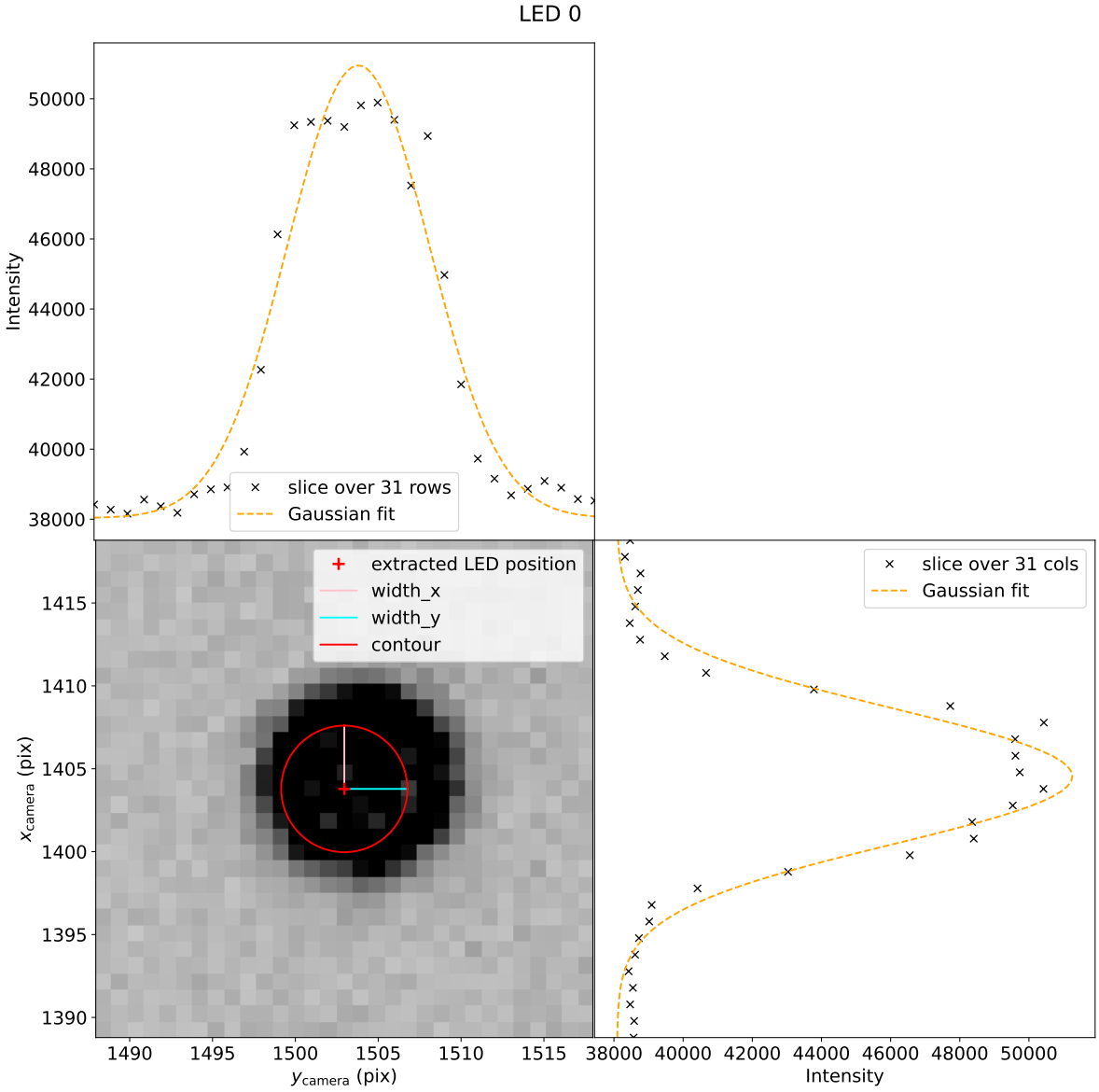

Figure 5: Intensity profile of LED 0 with non-normalized Gaussian distribution fitted and an ellipse indicating the width of the spot.

Noticeably the red ellipse, indicating the extracted position and width of the spot, seams to be slightly off. This offset will be analyzed in chapter 3.3.

In summary, using the spot extraction tool combined with the LED fitting tool, the LEDs on the camera body can be detected in the real pointing camera image. The

intensity profile per x and y axis can be approximated as a Gaussian distribution.

3 Simulation of pointing camera images

Using the information gathered in the previous section, we develop the simulations further, i. e. we simulate the camera body as well as the LEDs on top.
Later on, the resulting images will be validated by comparing them to real images.

3.1 Extension of pointing camera image simulation

Camera body

The first part of extending the night sky simulation is to model the shape of the camera body.

The geometry seen in real images is rectangular with many details. Currently, there is no necessity to model those details. Thus, a simple rectangle described by a width and a height is aligned to the camera body seen in the image.
The intensity of the rectangle is set homogeneously by the mean surface intensity of the camera body, determined from the real image. Therefore, only the mean value over the border pixels around the LED like in Figure 5 and over all LEDs is formed.
In reality the telescope structure blocks the light of the sky behind, so the pixel values of the simulated sky, where the camera body is located, are simply overwritten. Of course, the stars still contribute to the indirect illumination of the camera body. That is why the body has not zero intensity.

LEDs

The next step is to use the information about the characteristics of the LEDs acquired from chapter 2 to simulate them.
The intensity profile in the simulation does follow a Gaussian distribution. The width of the intensity is set by the mean value of the extracted width in both axes over all eight LEDs from the image shown in Figure 4. The width is equal for all LEDs. The total intensity of each individual LED is set to the extracted intensity of the spot at the corresponding position. However, the extracted positions are not used, but the nominal LED positions on the telescope structure. These are known by construction and assumed not to change over a short period of time, whereas the intensity can change rather rapidly due to a tilt of the telescope structure, aging process of the LEDs or dirt. It also provides the opportunity to validate the extraction algorithm, which will be discussed in a subsequent chapter.

At last, the intensity values of the LEDs are added to those of the simulated camera body.
It is also important to specify the same adjusted telescope pointing as the real image, since

the sky is dependent by that. Due to better comparison of the images, the start time and exposure duration of the real image are taken into account for the simulations.

Figure 6 shows the simulation to the image in Figure 4.

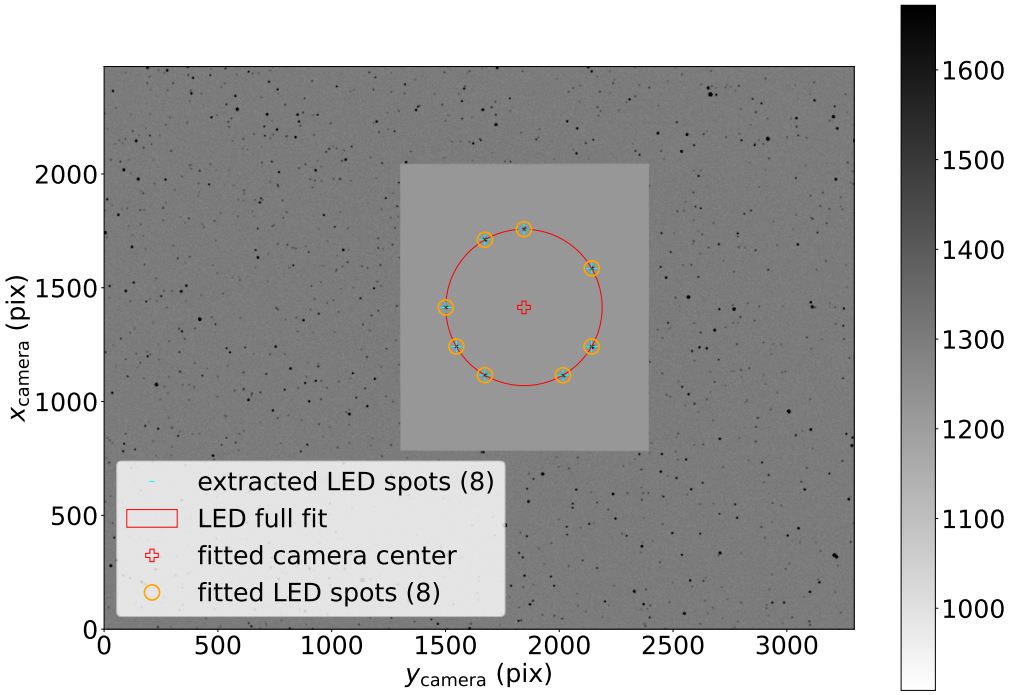

Figure 6: Simulation of the pointing camera image shown in Figure 4. The extracted spots on the camera body and the circle fitted to the LED spots are shown.

It is worth remarking, that the modelled camera body with the LEDs are in total flexibly translatable and rotatable due to the internal structure of the framework.

3.2 Comparison of simulation to real image

It is important to validate that the simulation adequately reproduces the pointing camera image well. Therefore, the real pointing image in Figure 4 is compared to the corresponding simulated image in Figure 6.

At first sight, the simulated shape of the camera body has adequately the same size and position as in the real image. Relative to the body, the LEDs are positioned and arranged as the ones visible in the real image.

Since the data provided by the analysis tools is crucial for determining the pointing, it is useful to apply the extraction and the fitting algorithm on the simulation, to compare the outcomes of both tools with those applied on the real image.

By applying the spot extraction tool on the simulation, while the sky is masked as for the real image in chapter 2, exactly eight spots are returned, which are the LEDs. The intensity of the area of the body is lower than the threshold used as criterion for the spot extraction, thus only the LEDs are detected. This is visible in Figure 6.

The position, width and total intensity of a spot provided by extraction of the real and the simulated image are opposed exemplarily for LED 0 in Table 2.

		real image	simulation
position(pix)	x	1749.99	1757.35
	y	1844.48	1844.89
width(pix)	x	3.97	4.40
	y	3.90	4.57
total intensity		206524.28	206586.98

Table 2: Position and width in x and y direction as well as total intensity of LED 0 provided by the spot extraction tool applied on the real pointing image in Figure 4 and the simulated pointing image in Figure 6.

Comparing the extracted spot coordinates of the simulation for all LEDs, the x coordinates do vary by about 4 to 10 pixels from the ones of the real image. Interestingly, the y coordinates do only vary by 1 to 3 pixels. Since there are statistical uncertainties bound to the extraction procedure, comparing whole series of images is necessary to describe those. From this comparison, it is only derived that the simulated positions of the LEDs are indeed in the surrounding of the positions taken from the real image.
Note, that the nominal LED positions are used for simulation, not the extracted ones from the real image. Since the offsets in the x coordinates have all the same direction, this could be a result of the camera support structure not being rigid but bendable, resulting in a shifted position in pointing images. This will be discussed in detail in chapter 3.3.

The total intensity of each LED does differ from the corresponding intensity from the

real images in the range of 0.002 % to 0.044 %. So the intensity of each simulated LED is comparable to the real ones.

Noticeably, the simulated LEDs have a slightly larger spatial extension on average, which is in the order of half a pixel. Compared to the radius of the LED spot of about 7 pix this is negligible and not relevant for the remaining comparison.
Still a possible reason could be, that the extraction algorithm does not estimate the background precisely, resulting in values at large distances contributing to the intensity distribution. Subsequently, this results in estimating the distribution with a greater width. This requires a close look into the spot extraction software.

Now the circle fitted by the LED positions in each of the real and simulated image can be compared, i. e. the position of the center with the resulting radius. The fitted parameters are recorded in Table 3.

		real image	simulation
center position (pix)	x	1406.09	1413.40
	y	1846.06	1844.96
radius (pix)		343.29	343.49

Table 3: Position and radius of the circle provided by the circle fitting tool applied on the real pointing image in Figure 4 and the simulated pointing image in Figure 6.

The center coordinates from both images do differ about 7 pixels in x direction and about 1 pixel in y direction. This also matches roughly with the differences in the extracted LED positions, which means, that a general offset in the extracted LEDs also causes a corresponding offset in the center position of the fitted circle.
Also, a general offset in the coordinates does not affect the radius of the circle, which reflects in the radii of the fits in the table.

For the sake of completeness, the sky can also be compared. It has already been shown, the simulation accurately reproduces observed star fields.[6]
It is also noticeable that the star field has a shift in positive y direction and negative x direction in the image. Possibly the pointing direction of the pointing camera is not aligned to the nominal telescope pointing, i. e. the orientation of the telescope dish adjusted by motors. The pointing of the camera can be determined by orientating along the stars seen in the pointing image. For the simulations, the nominal telescope pointing is used, thus resulting in a shifted star field.
However, this has no direct influence on the spot extraction and LED fitting tools, since the sky is masked out.

In summary, the simulated pointing camera images are reproducing the real images well, since the extraction and fitting tools are working fine on the simulations, delivering similar results on both the real and the simulated images.

As mentioned, the simulation software is creating images with statistical fluctuations, i. e. the Gaussian distributed intensity of the simulated LEDs incorporates randomness. Thus, simulating a real image twice will result in two slightly different images. This leads to different results by the spot extraction tool and subsequently by the circle fitting tool.

These statistical deviations will be analyzed in the next chapter.

3.3 Statistical analysis of real and simulated images

To perform a statistical analysis, many images are necessary. In particular, 100 real pointing camera images with 15 s exposure duration has been taken. Also, 100 images have been simulated with one common pointing direction.
In the following, these two series of images will separately be analyzed in terms of accuracy and precision of extracting the LED positions and fitting of the circle, i.e. the center position and radius, over many images. Simultaneously, the real series will be compared to the simulated similarly.

Therefore, the spot extraction and LED fitting tools are applied on each image as described in chapter 2. Non-LED spots, that can be detected especially in real images, are filtered by the LED fit algorithm. Thus, exactly eight LEDs are detected in all images, ensuring the comparability.

At last, the number of LEDs will be reduced to observe its influence on the LED fit.

Extracted to nominal LED position

Since the LEDs get simulated with nominal LED positions, the spot extraction algorithm can be validated by considering the error of the extracted LED spots relative to the nominal position per x and y axis.
The difference between the extracted position and the nominal position collected for all LEDs over the simulation series is represented as a normalized histogram for each axis in Figure 7.

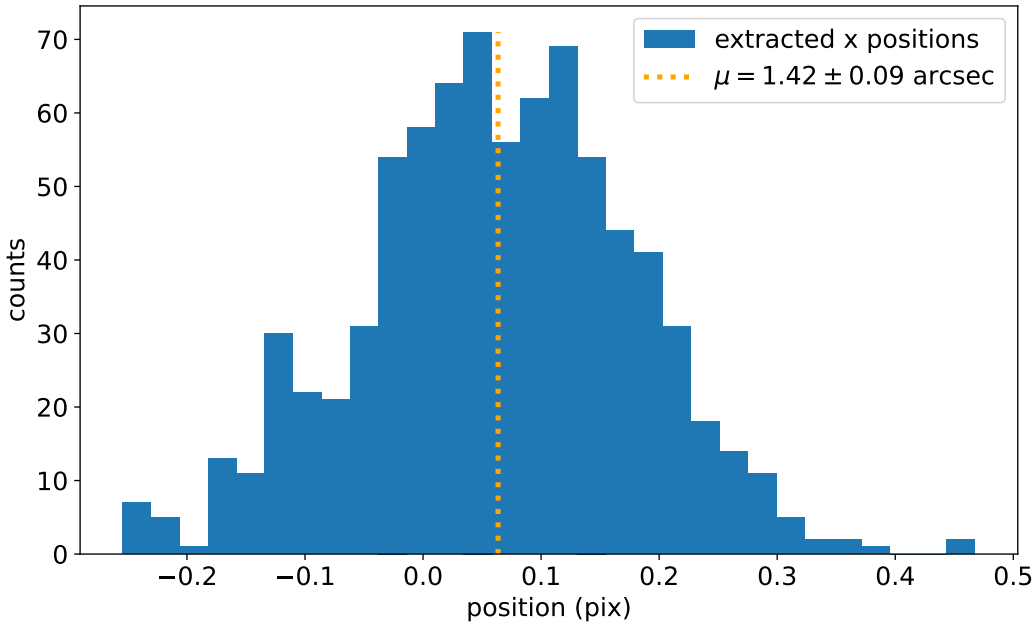

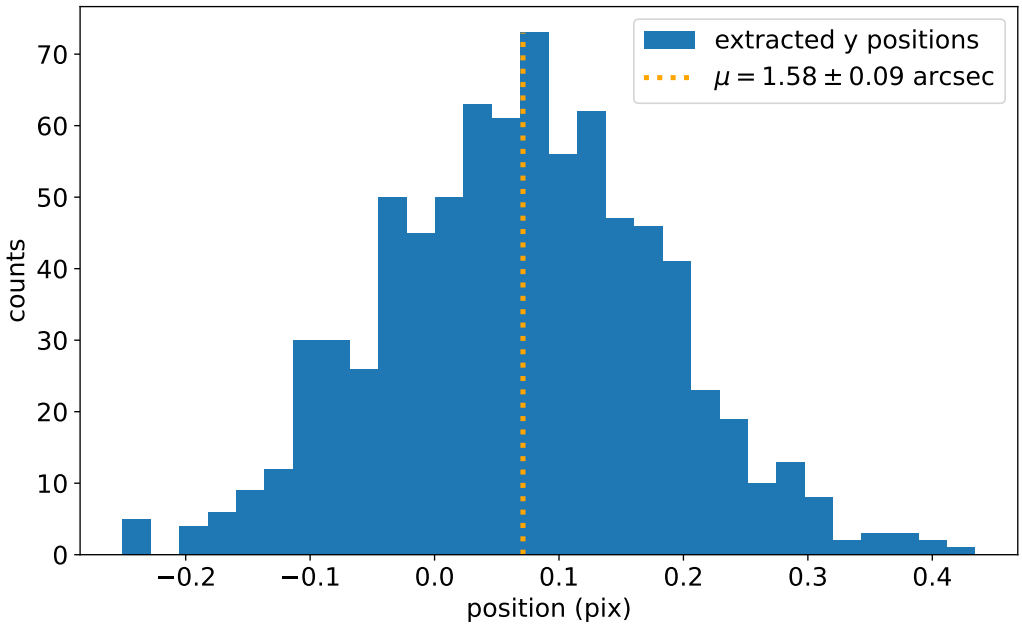

Figure 7: Histogram of the difference between the extracted LED positions in simulations and the corresponding nominal LED positions in x and y direction. The mean value μ of the distribution has the unit of seconds of arc.

The mean value and its error, as well as the standard deviation are calculated for that set of data.

Here, a mean value of 0 arcsec is expected, meaning that the extraction tool does return the correct LED position. But the mean relative position of about 1.5 arcsec per axis indicates a systematic offset in the extraction of the LED spots.
As this offset is in the order of 10^{-2} pix it can not be explained by some mismatching of pixel indices. This could possibly be an unknown source of systematic feature that needs to be investigated in more detail in the spot extraction software.

The spread of about 2.5 arcsec per axis is fulfilling the precision requirement of better than 7 arcsec for CTA telescopes.

Furthermore, the mean offset for each LED over the series is considered separately. The respective mean positions with standard error of the mean value per labeled LED are shown in Figure 8.

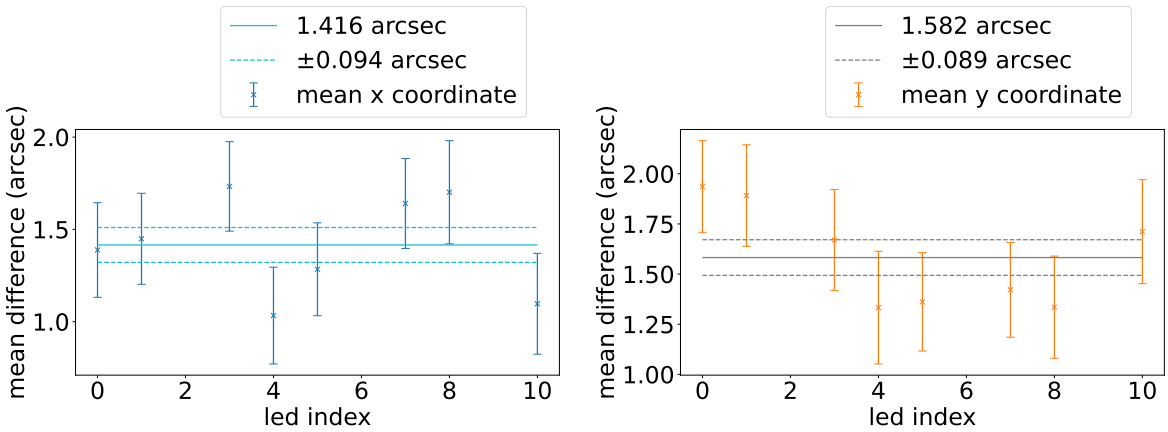

Figure 8: Mean offset of individual LEDs in simulated images in x and y direction with the standard error of the mean. The horizontal line represents the arithmetic average over the mean offsets of each LED. LED 2, 6, 9 and 11 are not operational hence do not contribute to the analysis.

The mean extracted position of each LED is distributed around the average position for all LEDs, mostly within the standard error of mean position of each LED.

Similarly, the series of real pointing images can be analyzed.

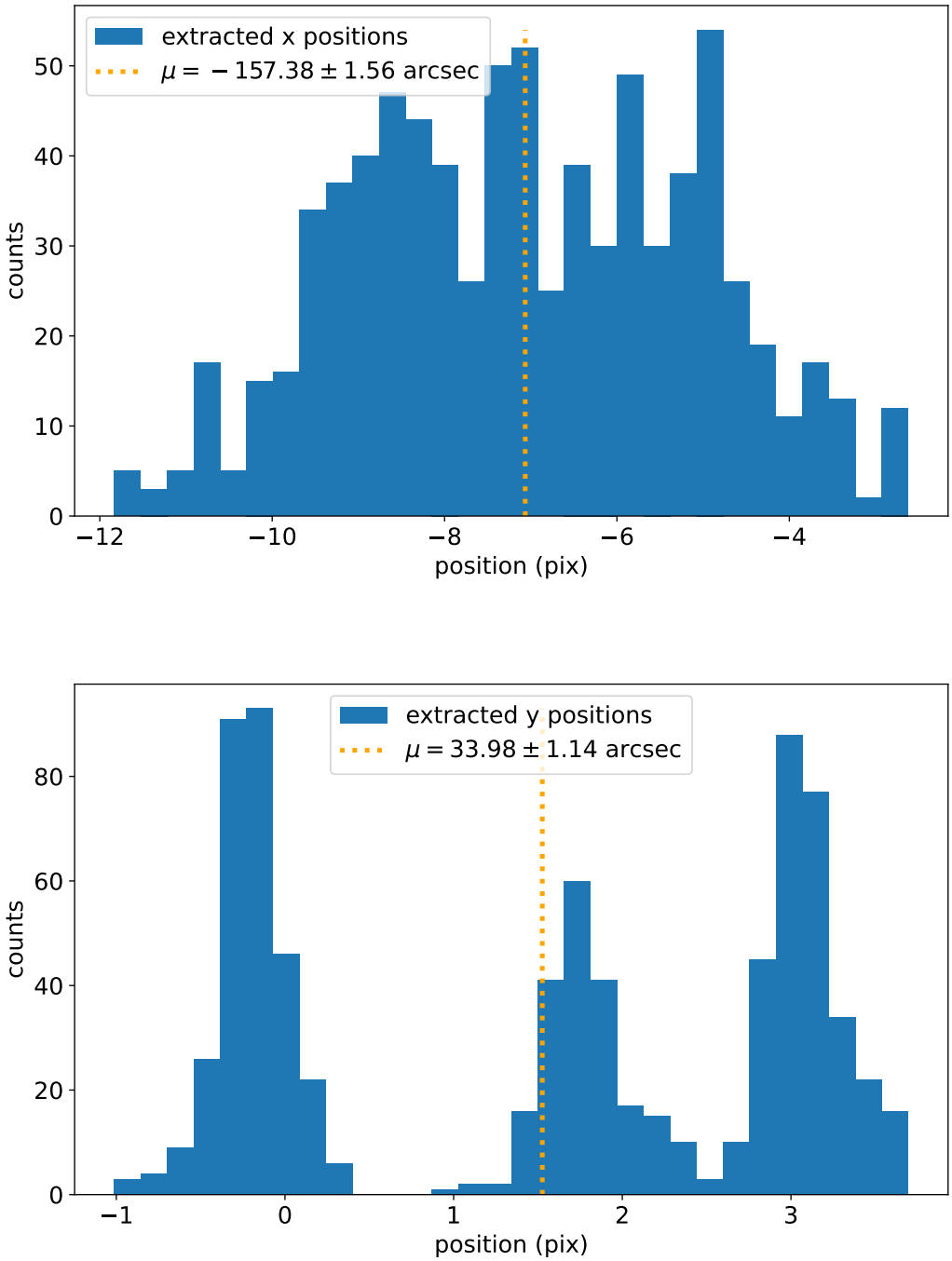

Figure 9: Histogram of the difference between the extracted LED positions in real images and the corresponding nominal LED positions in x and y direction. The mean value μ of the distribution has the unit of seconds of arc.

As seen in Figure 9, the extracted x coordinates of the LEDs are about 3-11 pix away from the nominal, which are up to about 200 arcsec. Defining the mean value and standard deviation of that dataset is less useful, because there do appear three individual peaks.

In this case, the statistical fluctuation of the spot extraction is dominated by the deformation of the camera support structure due to movement of the telescope between image takings.
The more shallow the angle of the telescope pointing over the ground, the more gravitational force is applied on the structure arms and the more the structure gets bend. This results in a shifted position of the camera and the LEDs in the pointing camera frame, particularly in negative x direction, which is true in the figure.
This can also been seen in the mean offset of each individual LED in Figure 10. There are LEDs with an average offset to the nominal position in x direction of up to 2 times as of other LEDs.

Considering the y coordinates, there are three discrete peaks. A possible explanation is that moving the telescope in altitude direction does often imply a lock in azimuth direction. This would reflect in the mean offset for each individual LED, which is shown in Figure 10.

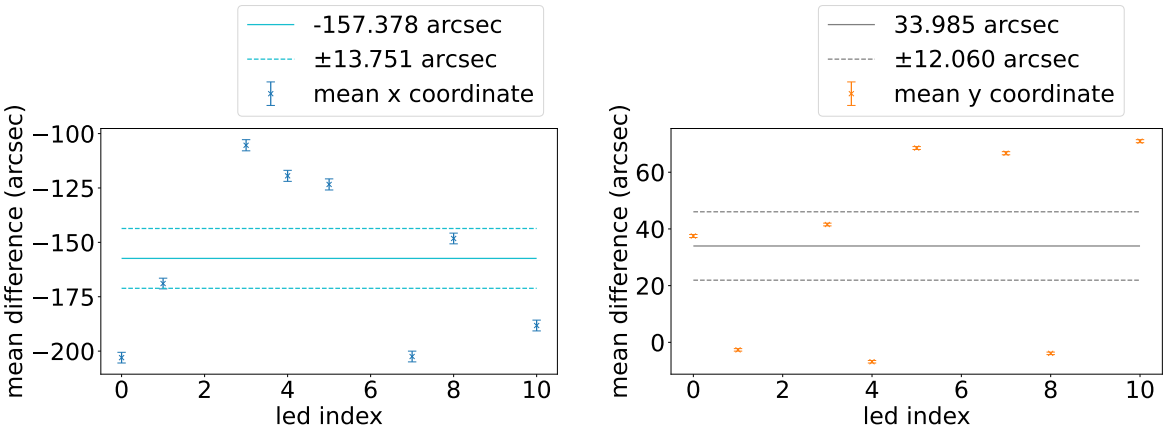

Figure 10: Mean offset of individual LEDs in real images in x and y direction with the standard error of the mean. The horizontal line represents the arithmetic average over the mean offsets of each LED. LED 2, 6, 9 and 11 are not operational hence do not contribute to the analysis.

A lock in azimuth direction would be visible as the LEDs having all the same mean offset in y direction. Instead, each LED has a different average offset to the nominal y coordinate. In fact, multiple LEDs share a common offset position, forming the discrete peaks in the

histogram.
A lock in azimuth direction is not the main reason for this observation. It is also possible that the LEDs on the telescope are installed with a slight shift. The offset of about 60 arcsec seen in Figure 10 could correspond to a shift in LED position of about 3 mm on the telescope, which is of realistic order.

Center of LED fit

Since the extracted LED positions have an offset, it is assumable to find that same offset on the average center position of the fitted circle.
The difference between the fitted center coordinates and the nominal center coordinates for the simulations is shown as a histogram in Figure 11. The nominal center position is defined by the circle aligned to the nominal LED positions.

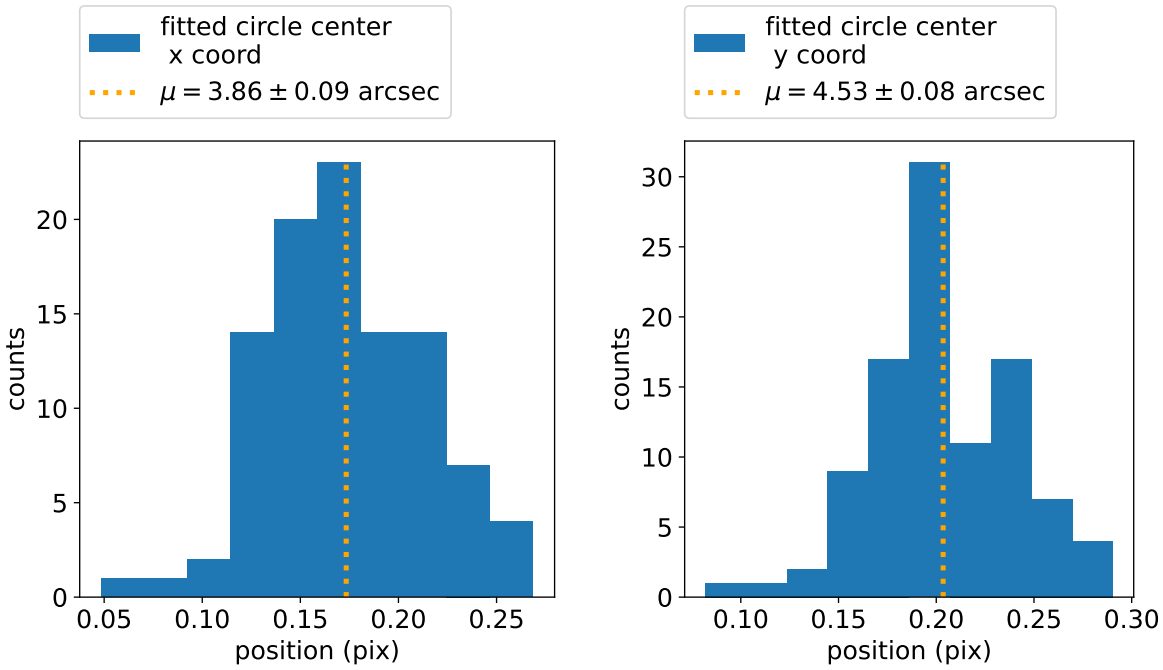

Figure 11: Histogram of the difference between the circle center fitted to the extracted LED positions in simulated images and the corresponding nominal center position in x and y direction. The mean value μ of the distribution has the unit of seconds of arc.

Apparently, there is an offset of the fitted to the nominal center position about 3 times as high as the offset for the LED positions. This means that besides the offset by the spot extraction, there is a currently unknown source of additional shift while fitting the circle

to the LED positions.

The standard deviation for the fitted center position is defined as $\sigma_{\mathrm{LED}}/\sqrt{n_{\mathrm{LED}}}$ with the standard deviation σ_{LED} for the extracted LED positions to the nominal positions and the number of LEDs n_{LED} used for the fitting. The spread of the center position of about 0.9 arcsec per axis perfectly approves the assumption and accomplishes the precision requirement of better than 7 arcsec for CTA telescopes.

In comparison, taking a look at the distribution of the center position for real images in Figure 12, it appears that the general offset of about -150 arcsec in x and about 34 arcsec in y direction on average does roughly match the offset for the LED positions. The positions do also spread widely, especially in x direction, due to the movement of the telescope between images.

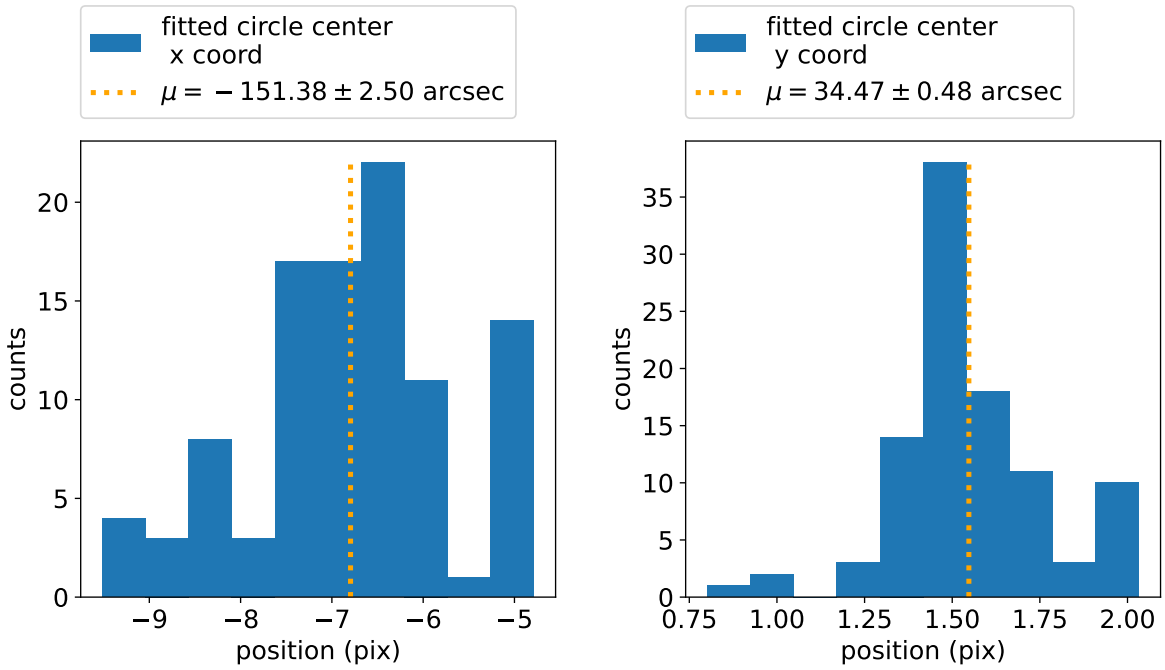

Figure 12: Histogram of the difference between the circle center fitted to the extracted LED positions in real images and the corresponding nominal center position in x and y direction. The mean value μ of the distribution has the unit of seconds of arc.

In Figure 13 the camera center fitted in individual real images is plotted over the starting time of the image exposure.

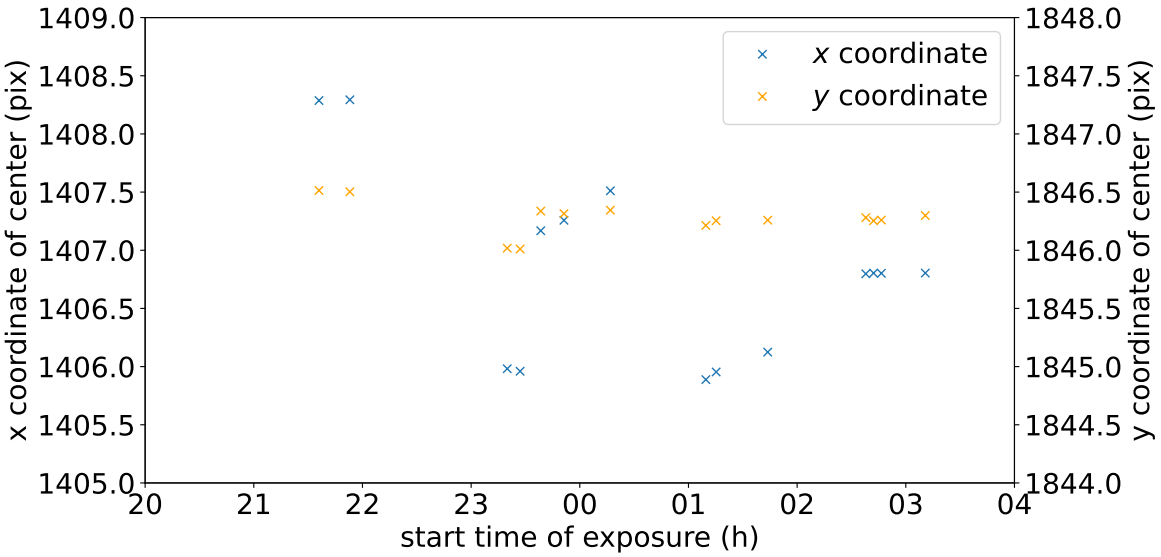

Figure 13: Movement of the fitted circle center in real images for different start times of the exposure of the pointing camera within a night.

While the center does only move by about 0.6 pix, which are 13.2 arcsec, in y direction, the shift in x direction is about 2 pix or 44 arcsec. This is caused by the bending of the telescope structure, thus the telescope has switched to different pointing directions within a night. Images taken within short times intervals of less than an hour tend to not change drastically in the camera center, thus the telescope was likely not moved in short periods of time.

Radius of LED fit

The position of the LEDs relative to each other should be the same for both the real images and the simulated images. Thus, the radii of the LED fit should be the same, which are recorded in 4.

		real images	simulated images
mean radius	(pix)	343.305 ± 0.022	343.476 ± 0.004
standard deviation	(pix)	0.022	0.043

Table 4: Comparison of the mean radius of the circle fitted to the extracted LED positions for real and simulated pointing image series.

Indeed, the mean radius is adequately identical in both image series with sufficient preci-

sion.
Interestingly, the standard deviation for the radius in simulated images is greater than in real images. The reason for that is currently unclear.

Also, the residuum of the LED spots to the circle can be considered in Figure 14. This is determined by the distance of the spot to the circle center minus the radius of the circle.

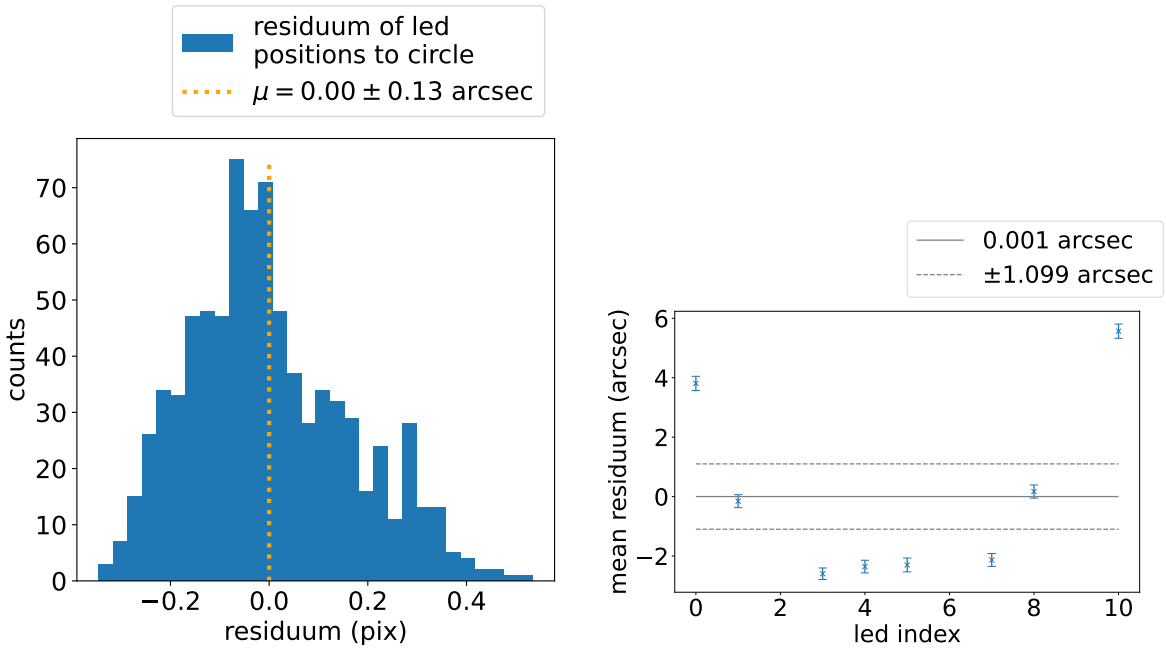

Figure 14: Histogram of the residuum of the extracted LED positions to the fitted circle for simulated images with the mean residuum μ (left) and the mean residuum of each LED (right). The horizontal line indicates the average over the mean residua of each LED.

On average, the extracted spots of the simulated LEDs are almost perfectly on the circle, but their spread of about 3.7 arcsec requires a look at the residuum of individual LEDs also in Figure 14.
Apparently, the LEDs 3 to 7 are more inside the circle. LED 1 and 8 have a residuum of about 0 arcsec and the remaining LEDs 0 and 11 are rather outside the circle. It appears like the circle is shifted, resulting in LEDs being inside the circle and the ones on the opposite side of the circle outside. However, the observed shift of the center position in this chapter before points in the other direction.
Further investigations need to be done in order to understand this phenomenon.

Similarly, the residuum can be analyzed for real images, which is shown in Figure 15.

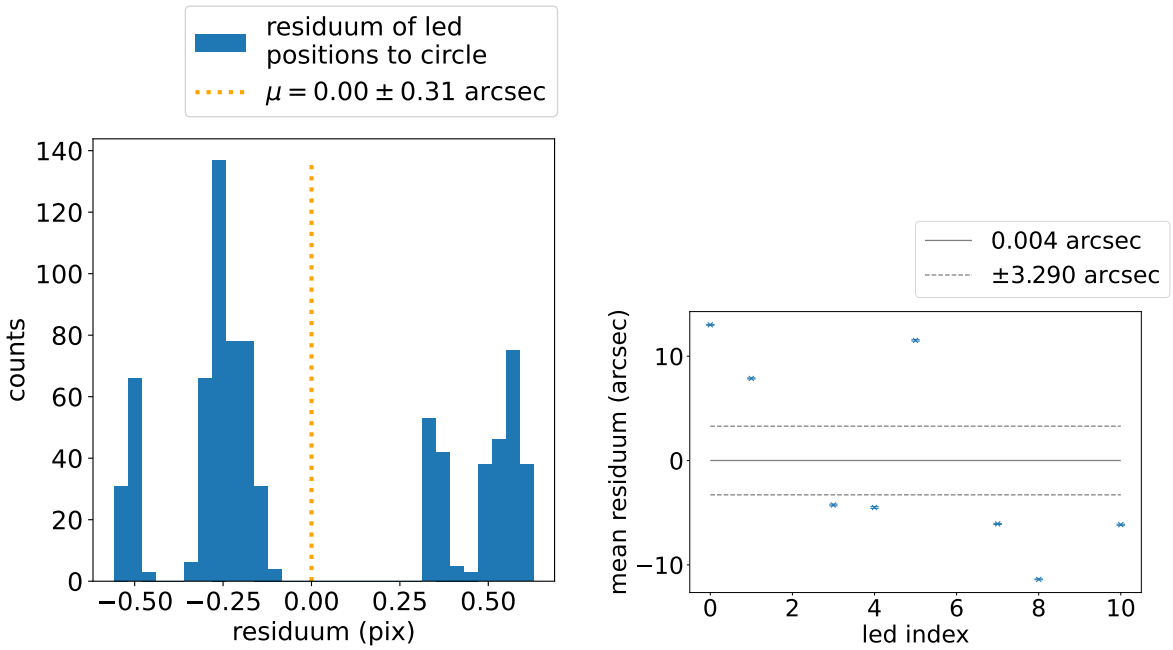

Figure 15: Histogram of the residuum of the extracted LED positions to the fitted circle for real images with the mean residuum μ (left) and the mean residuum of each LED (right). The horizontal line indicates the average over the mean residua of each LED.

The spot positions of the real LEDs are distributed among discrete peaks with distances up to 0.6 pix to the circle and a main peak at about -0.25 pix.

It is possible that the distance of the LEDs to the circle varies by thermal expansion of parts of the telescope. The roughly approximated ratio of the residua to the circle radius is about 1/1000. Thus, an extension of structures on the telescope by this ratio would be sufficient to change the LED position relative to the circle.
Since the images are taken on different nights within a month, the thermal expansion can not be considered constant for all images, which would result in widely spread distributions of the residuum for each LED if this would be the main reason. This is not the case in 15. But multiple LEDs are sharing common residua similarly to the extracted LED positions. The possibility that the LEDs are installed with slight shifts on the telescope could be a sufficient explanation.

On average, the mean residua of the individual LEDs do balance themselves around

the circle, with an error of about 1 arcsec for the simulated images and 3 arcsec for the real images.

In this chapter, it was found, that the extracted spot positions contain a systematical offset.
Also, the circle fitted to the LED positions shows an offset, which is still to be determined. The distance of the LED positions to the circle is on average zero, but the individual LEDs are distributed around the circle, especially in real images.
Additionally, the movement of the telescope and the resulting bending of the camera support structure are observed.

3.4 LED fitting with 3 LEDs compared to 8 LEDs

The number of operating LEDs has an influence on the determination of the telescope pointing, i. e. on the LED fit.
As for the MAGIC telescope, originally twelve reference LEDs are installed, but only eight are operational in the images taken for this thesis. The reduction of LEDs can be imitated by disregarding LEDs selectively. The results of the LED fit are then compared between the case of eight LEDs and the case of fewer LEDs.

The minimum number of spots required for a well-defined circle is three. Therefore, it is a suitable boarder case to reduce the number of LEDs to three, i. e. discarding the extracted LED positions that should not be taken into account for the LED fit. In the following two constellations of three LEDs on the circle are considered, i. e. a symmetrical and an asymmetrical, which are both shown in Figure 16.

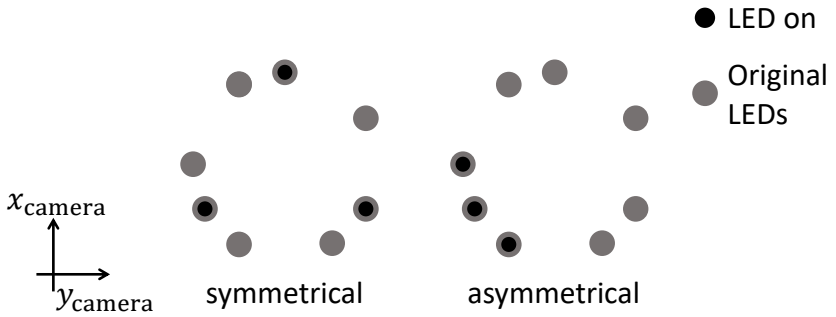

Figure 16: Draft of using three LEDs in a symmetrical and an asymmetrical constellation. Originally, eight LEDs are operative.

The resulting center positions and radii of both constellations are then compared to the respective series with the complete set of eight LEDs.

Shift of the fitted circle center

		symmetric	asymmetric
mean shift (arcsec)	x	0.116 ± 0.123	-2.590 ± 0.332
	y	-0.039 ± 0.118	-3.817 ± 0.372
standard deviation (arcsec)	x	1.233	3.317
	y	1.182	3.722

Table 5: Comparison of the mean shift of the circle center between being fitted to eight LEDs and a fit to three LEDs arranged symmetrically and asymmetrically for simulated images.

For the simulations, the fitted circle center with three symmetrically arranged LEDs and with eight LEDs is adequately the same, as shown in Table 5. The standard deviation matches the expectation, that it follows $\sigma_{\mathrm{LED}}/\sqrt{n_{\mathrm{LED}}}$ with $\sigma_{\mathrm{LED}} \approx 2.5\,\mathrm{arcsec}$, the precision of the spot extraction procedure for the LEDs.

For the asymmetrical constellation, there is a great shift in the center position. Here, the uncertainty of the extracted LED position has a significant influence on the circle fit, meaning slightly shifted LEDs can cause a significant shift of the circle position. Especially, the arrangement orientated to one side of the image causes a shift in the same direction. That is because the LED fitting tool is fitting the circle based on the intensity distribution of each LED. In the asymmetrical constellation, the intensity overall three LEDs is clustered, thus causing a shift towards the cluster. This is illustrated in Figure 17. Therefore, also the precision decreases.

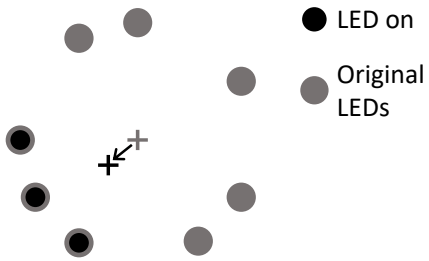

Figure 17: Schematic shift of the circle center from fitting to eight LEDs towards the asymmetrical arrangement of three LED.

The same comparison can be done for real images. The shifted center positions are recorded in Table 6.

		symmetric	asymmetric
mean shift (arcsec)	x	1.650 ± 0.031	-15.522 ± 0.106
	y	3.341 ± 0.030	7.496 ± 0.100
standard deviation (arcsec)	x	0.308	1.056
	y	0.301	0.997

Table 6: Comparison of the mean shift of the circle center between being fitted to eight LEDs and a fit to three LEDs arranged symmetrically and asymmetrically for real images.

Again, the asymmetrical constellation results in a greater shift and lower precision of the circle center than the symmetrical.

Interestingly, the offset of the symmetrical arrangement in the real images is significantly greater than in the simulated images. This could also be related to a thermal expansion of the telescope structure. The same holds respectively for the asymmetrical case. Whereas for both arrangements the precision of the center is each better for the real series than the simulations.

To understand this, it is useful to consider the correlation between the camera center fitted by three LEDs and by eight LEDs. Both constellations of three LEDs are considered for the real and simulated images separately.

Correlation of the center position

Figure 18 shows the correlation of the center position for the symmetrical and asymmetrical constellation in simulated images.
The center positions per axis for eight LEDs are about 50-60 % correlated with the center for the symmetrical arrangement of three LED. The mean value of each coordinate pair has adequately no offset to the diagonal, which matches the observation, that there is almost no shift of the camera center in this case.
The strength of correlation is dominated by the statistical uncertainties of the circle fit. These are indicated by the error bars.

In comparison, the center position using the asymmetrical constellation is almost uncorrelated. That originates in the greater spread and uncertainty of the center position with three LEDs, as described before. Also, the offset seen in Table 5 is clearly visible in the mean value.

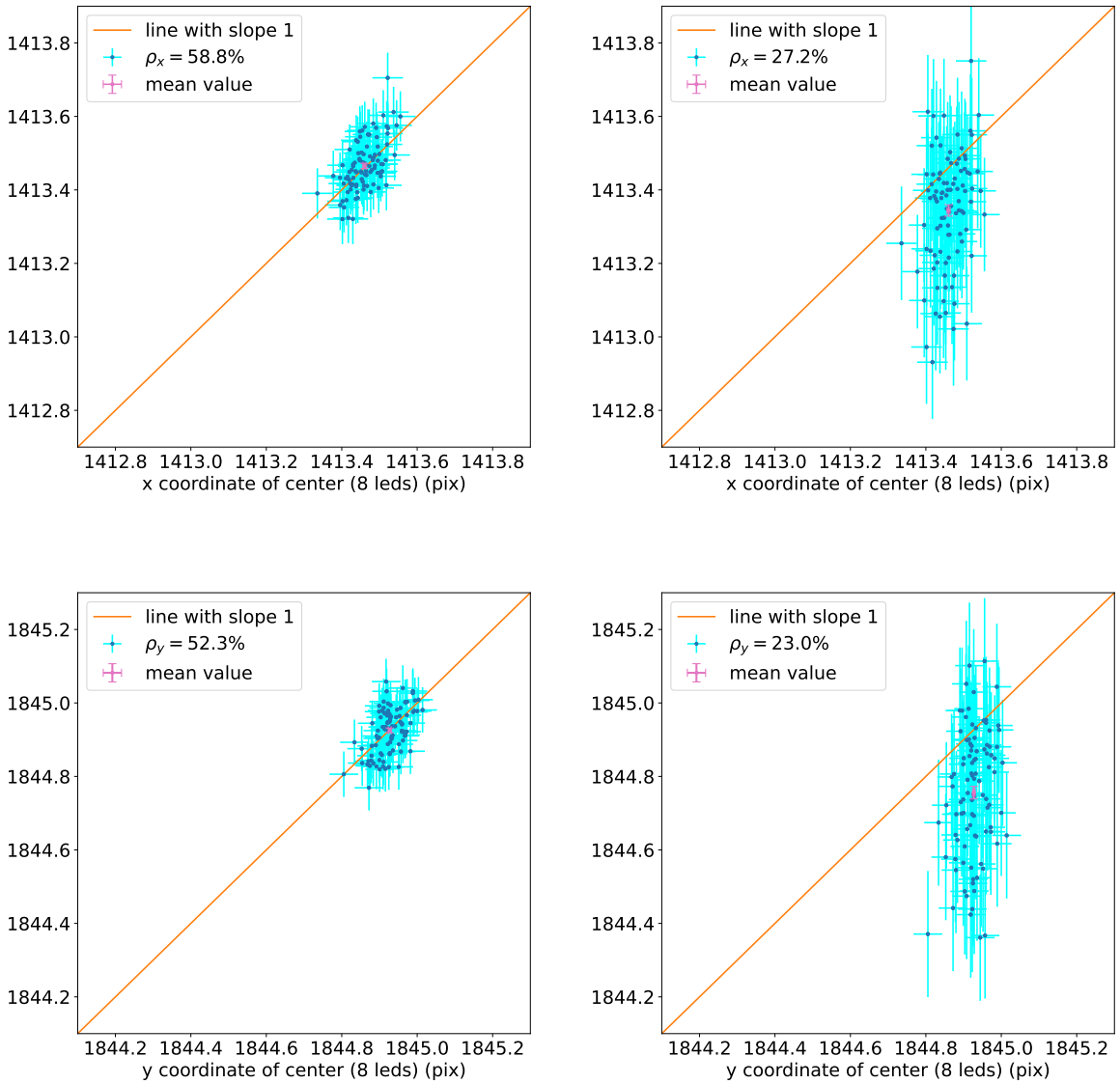

Figure 18: Correlation between the position of the camera center fitted to eight LEDs and to three LEDs arranged in symmetrical (left) and asymmetrical constellation for simulated images. The x and y coordinates of the center position are considered separately. For better comparison, all plots are scaled uniformly.

On first sight, the center positions in the real images (Figure 19) are perfectly correlated for each constellation. But the movement of the center positions happens on a greater scale in the plots. The correlation shows the movement of the camera center due to deformation

of the support structure.
In case of the asymmetrically arranged three LEDs, the greater offset by the constellation is already visible on these scales.

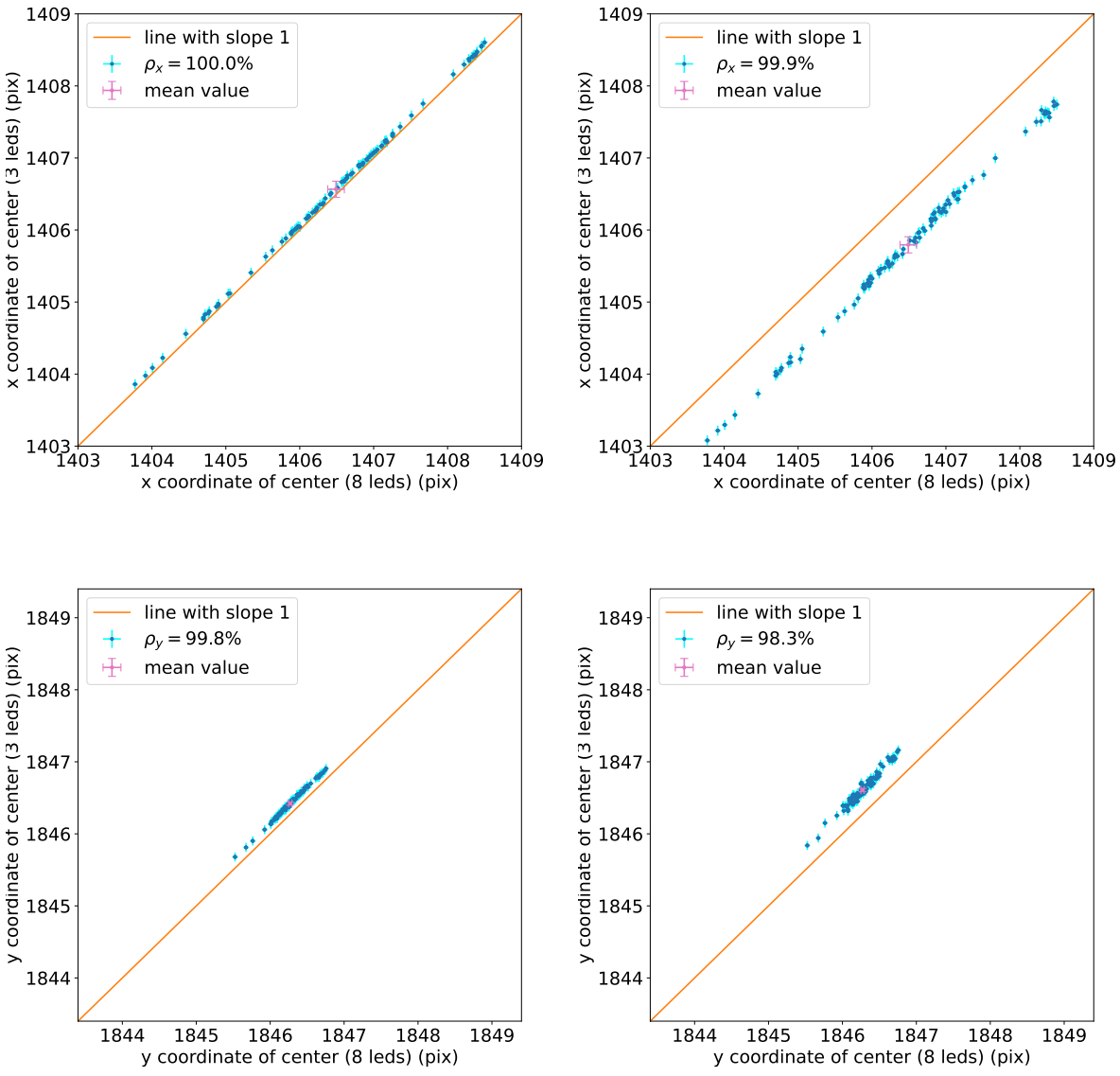

Figure 19: Correlation between the position of the camera center fitted to eight LEDs and to three LEDs arranged in symmetrical (left) and asymmetrical constellation for real images. The x and y coordinates of the center position are considered separately. For better comparison, all plots are scaled uniformly.

Changes on the circle radius

In addition to the shift of the center positions also the radius of the circle changes, which you can tell from Table 7 for simulated images and Table 8 for real images.

		8 LEDs	3 LEDs	
			symmetric	asymmetric
mean radius	(pix)	343.476 ± 0.004	343.500 ± 0.007	343.179 ± 0.018
standard deviation	(pix)	0.043	0.066	0.179

Table 7: Comparison of the mean radius of the circle center fitted to eight LEDs and to three LEDs in symmetrical and asymmetrical constellation for simulated images, including the standard deviation of the fit.

		8 LEDs	3 LEDs	
			symmetric	asymmetric
mean radius	(pix)	343.305 ± 0.022	343.262 ± 0.003	343.290 ± 0.005
standard deviation	(pix)	0.022	0.027	0.045

Table 8: Comparison of the mean radius of the circle center fitted to eight LEDs and to three LEDs in symmetrical and asymmetrical constellation for real images, including the standard deviation of the fit.

Especially for the asymmetrical case, the shift of the center towards the LED cluster results in a reduction of the radius.

Considering Table 8, the radius for the real images, fitted to the asymmetrical constellation, does not change considerably, while the corresponding center position has a significant shift (see Table 6), suggesting a shift of the circle in total.
Since the three LEDs do not change their position while discarding the other five, that is not caused by an offset in the LEDs. Instead, the camera support structure with the LEDs can have a slight tilt against the pointing camera. Thus, the circle of LEDs would appear as an ellipse in the pointing camera frame. Since the LED fit implements fitting a circle, this can cause deviant radii and circle positions, especially for the asymmetrically arranged LEDs, because there is no opposing spot limiting the fit.

As for eight LEDs, the residuum of the LED position to the fitted circle can be considered for the case of three LEDs in both constellations. Since the construction of a circle by three spots is well-defined, the position of each individual LED is expected to be on

the circle, i. e. residuum about zero.

In Figure 20 the histogram of the residua of all three LEDs and the respective residuum of each LED are shown for both constellations in simulated images.

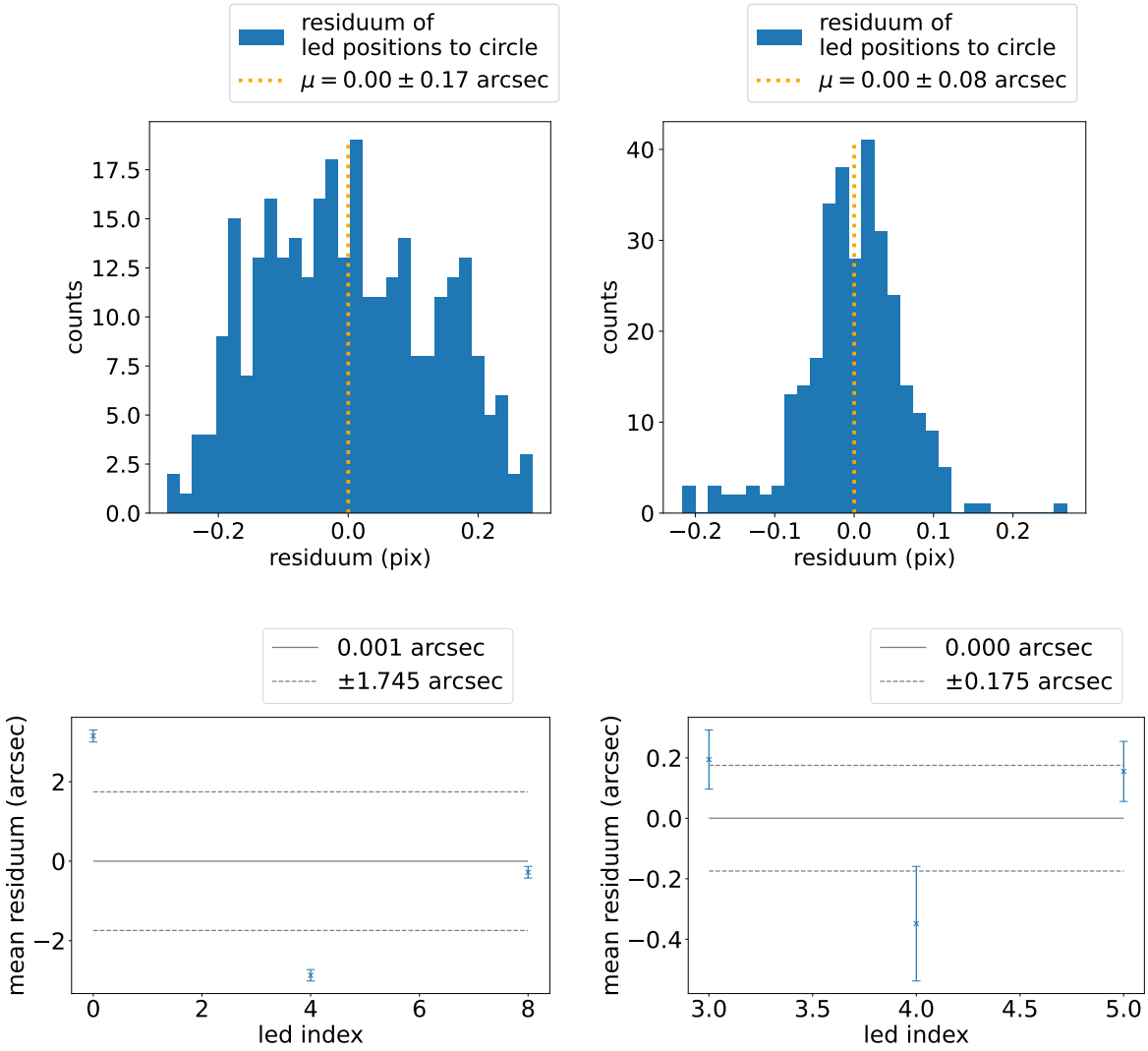

Figure 20: Histogram of the residuum of the extracted LED positions to the fitted circle for three LEDs in symmetrical (left) and asymmetrical constellation (right) in simulated images with the mean residuum μ and the mean residuum of each LED. The horizontal line indicates the average over the mean residua of each LED.

The overall mean residuum is in fact adequately 0 arcsec for both constellations, however the individual LED positions are not perfectly on the circle, but have distances of multiple seconds of arc for the symmetrical case.
A similar behavior of the individual LED positions is visible for the respective real images in Figure 21.

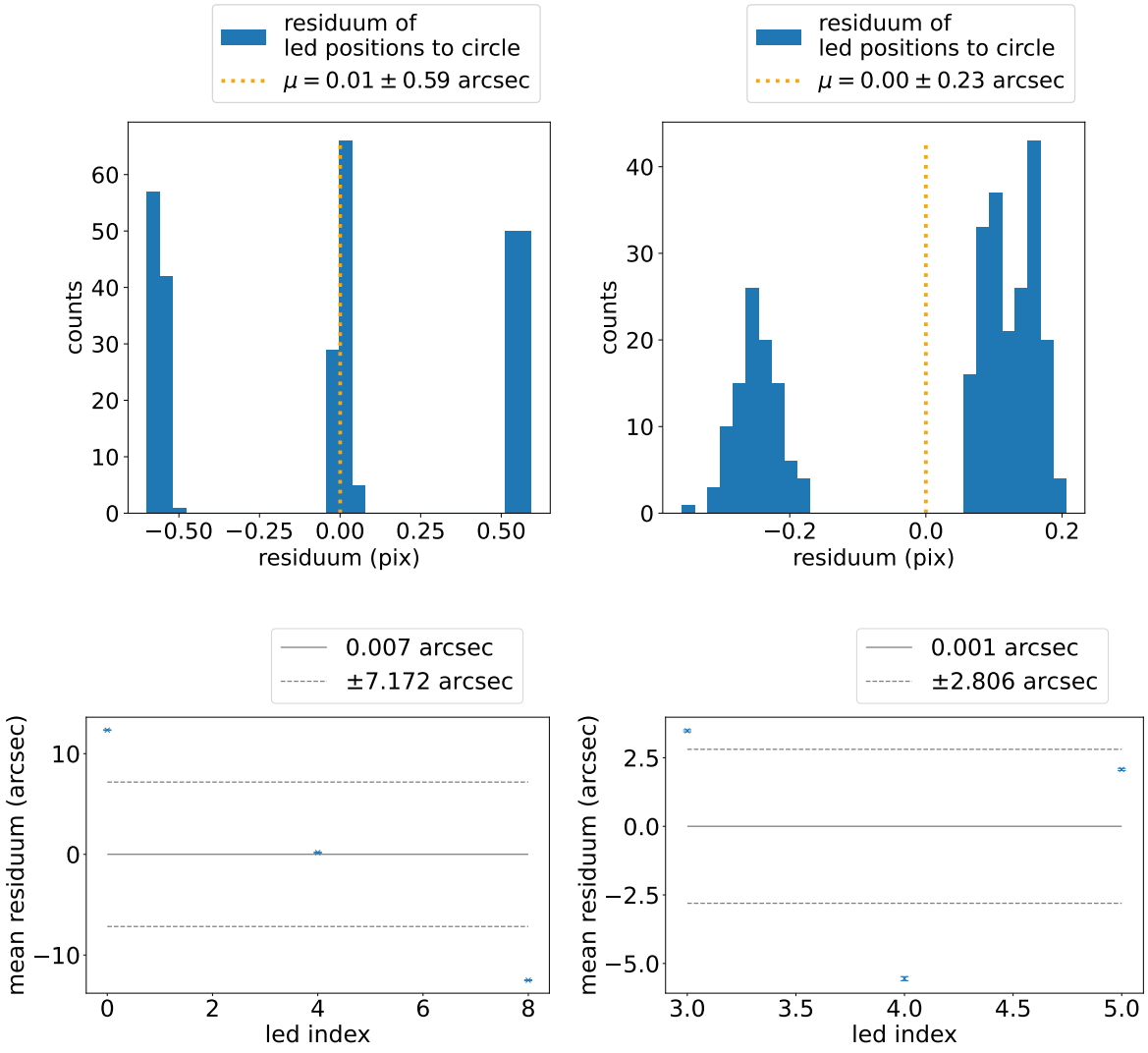

Figure 21: Histogram of the residuum of the extracted LED positions to the fitted circle for three LEDs in symmetrical (left) and asymmetrical constellation (right) in real images with the mean residuum μ and the mean residuum of each LED. The horizontal line indicates the average over the mean residua of each LED.

In addition, the distance of the LEDs to the circle is greater than for the simulations with discrete peaks appearing in the histograms.

A suggestion to the observed distances to the circle is, that the radius is fitted correctly, since the radius does not change drastically for three LEDs compared to eight, but there appears an offset in the center position resulting in a shifted circle and thus resulting in LED positions no longer aligned to the circle.
For the symmetrical cases, there is one LED in each image series where this possible shift happens along an axis with no significant impact on that LED.

To summarize this chapter, the number as well as the constellation of the LEDs have influence on the LED fit.
Using three LEDs for fitting the circle instead of eight does decrease the precision of determining the circle center.
Also, the asymmetrical constellation of the three LEDs reveals additional sensitivity to uncertainties in the LED positions compared to the symmetrical constellation.

4 Summary and conclusion

The framework for simulating pointing camera images for the CTA MST is extended by simulating the Cherenkov camera support structure with reference LEDs arranged in a circle around the Cherenkov camera. The LEDs are simulated with a Gaussian distributed intensity.
The simulated images reproduce real pointing images adequately.

In order to determine the telescope pointing precisely, the LEDs in real and simulated images are detected by the spot extraction algorithm and then used to fit a circle, which is determined by the LED positions. Both tools are provided by the Offline MST telescope pointing pipeline prototype for CTA.
The center position of the circle can be determined with a precision of less than 1 arcsec, which is satisfying the requirement of better than 7 arcsec for CTA telescopes.

Furthermore, a systematic offset of about 0.06 pix or 1.5 arcsec per axis for the extraction of LED positions is observed. The exact source of this offset is to be investigated further. A first step is to check the spot extraction algorithm for possible biases.

Since the Cherenkov camera with the LEDs can be tilted against the pointing camera, the circle of LEDs might appear as an ellipse. As shown in this thesis, it is necessary to extend the LED fit, which currently is fitting a circle, to fitting an ellipse.

The analysis of multiple real pointing images taken on the MAGIC telescope at different times and telescope pointing directions reveals that the camera support structure gets bend at different positions, likely due to gravitational forces. This results in a movement of the camera center in the image frame, especially in altitude direction.

Finally, the number of the reference LEDs is crucial for the determination of the Cherenkov camera center. The more spots are used for fitting the circle, the less the influence of the uncertainty of the individual spot positions, thus increasing the precision of the center position.
Also, the study has shown that a symmetrical arrangement of the LEDs on the circle delivers more precise results than for an asymmetrical constellation.

One of the applications of simulated pointing camera images is to develop and improve algorithms for sophisticated analysis methods. The offset in the results of the spot extraction is an important discovery. The spot extraction tool is the first component of the simulation and analysis chain thus it is important to be improved in the future.

5 References

[1] HESS Collaboration: Localizing the VHE γ-ray source at the Galactic Centre. *Monthly Notices of the Royal Astronomical Society*. Volume 402. Issue 3. March 2010. Pages 1877–1882. URL: https://doi.org/10.1111/j.1365-2966.2009.16014.x

[2] CTA Observatory. URL: https://www.cta-observatory.org

[3] MAGIC (telescope). URL: https://en.wikipedia.org/wiki/MAGIC_(telescope)

[4] Heitler, W.: Quantum theory of radiation. 1954.

[5] Tiziani, D.: The first analysis of very-high-energy gamma rays from the Large Magellanic Cloud with a novel analysis technique. PhD thesis. Friedrich-Alexander-Universität Erlangen-Nürnberg. 2020.

[6] Egelkraut, M.: Analysis and Improvement of the Single-CCD Pointing-Image Simulation. BSc thesis. Friedrich-Alexander-Universität Erlangen-Nürnberg. 2019.

[7] Cherenkov, P. A.: Visible Radiation Produced by Electrons Moving in a Medium with Velocities Exceeding that of Light. 1937. In: Physical Review 52, pp. 378–379.

[8] Offline MST telescope pointing pipeline prototype for CTA. In private collection by Prof. Dr. Christopher van Eldik. Erlangen Centre for Astroparticle Physics. Friedrich-Alexander-Universität Erlangen-Nürnberg.
URL: https://gitlab.com/vaneldik/ctapointing

[9] J.A. Hinton, W. Hofmann: Teraelectronvolt Astronomy. 2009. In: Annual Review of Astronomy & Astrophysics, vol. 47, Issue 1, pp.523-565.
URL: https://ui.adsabs.harvard.edu/link_gateway/2009ARA&A..47..523H/
doi:10.1146/annurev-astro-082708-101816

Danksagung

An dieser Stelle möchte ich mich bei Allen bedanken, die mich bei dieser Bachelorarbeit unterstützt haben. Mein besonderer Dank geht an:

- Prof. Dr. Christopher van Eldik für die Vergabe des spannenden Themas und die überaus informativen und aufregenden Gespräche jeden Mittwoch oder auch spontan zwischendurch.
- Dr. Andreas Specovius, der mir gerne meine Fragen beantwortet hat, diese Arbeit Korrektur gelesen hat und besonders gegen Ende der Arbeit nochmal lange Diskussionen zu den Inhalten mit mir führte.
- Frederik Wohlleben, der den einsamen Alltag im Büro durch lustige Unterhaltungen aufhellte und stets nützliche Tipps parat hat.

Eidesstattliche Erklärung

Hiermit bestätige ich, dass ich diese Arbeit selbstständig und nur unter Verwendung der angegebenen Hilfsmittel angefertigt habe.

Erlangen, den 12. August 2022

Martin Hein